Quaternary International 616 (2022) 1–11

Contents lists available at ScienceDirect

Quaternary International

journal homepage: www.elsevier.com/locate/quaint

MIS 13 and MIS 11 aggradational successions of the Paleo-Tiber delta: Geochronological constraints to sea-level fluctuations and to the Acheulean sites of Castel di Guido and Malagrotta (Rome, Italy)

Fabrizio Marra [a,*], Alison Pereira [b,c], Giovanni Boschian [d,e], Sébastien Nomade [f]

[a] Istituto Nazionale di Geofisica e Vulcanologia, Rome, Italy
[b] Université Paris-Saclay, CNRS UMR 8148, GEOPS, Rue du Belvédère Bât 504, F-91405, Orsay, France
[c] Département Hommes et environnements, Muséum National d'Histoire Naturelle, Paris, France
[d] Dipartimento di Biologia, Università di Pisa, Pisa, Italy
[e] Palaeo-Research Institute, University of Johannesburg, Auckland Park, Johannesburg, South Africa
[f] CEA Saclay, LSCE, UMR-8212, UVSQ-IPSL et Université Paris Saclay, Bât 714 Orme des Merisiers, 91190, Gif-sur-Yvette Cedex, France

ARTICLE INFO

Keywords:
MIS 11 highstand
Glacial termination V
Aggradational successions
Sea-level oscillations
Castel di guido
Central Italy

ABSTRACT

This contribution presents an application of the conceptual model of 'aggradational succession' (i.e., the sedimentary record deposited in response to sea-level rise during the glacial terminations) to a series of geological sections of the Paleo-Tiber delta cropping out along the Via Aurelia near Rome, Italy. The geochronological constraints provided here through $^{40}Ar/^{39}Ar$ dating of volcanic layers intercalated within the sedimentary deposits of the MIS 13 and MIS 11 aggradational successions resulted in some remarkable outcomes:

1) we reconstruct an independent chronology of the Mediterranean sea-level oscillations 450 through 380 ka, in good agreement with the $\delta^{18}O$ and the Red Sea relative sea level curve chronology;

2) the Glacial Termination V is here bracketed in the interval 423.1 ± 4.4–438.7 ± 1.2 ka;

3) we show that the aggradational successions of MIS 11 and MIS 13 display similar spatial/geometric features despite the significantly different amplitude of their Oxygen isotope records, challenging the regression models linking absolute values of benthic foraminifera $\delta^{18}O$ and ice-volume;

4) we show the relevance of a climatic-stratigraphic approach in dating coastal-to-fluvial sedimentary contexts;

5) we provide indirect age constraints with the precision of a few ka for two important palaeoanthropological and archaeological sites in central Italy bearing Acheulean lithic industries and human remains.

1. Introduction

The conceptual model of 'aggradational succession' has been widely used in literature to provide age constraints to the Middle-Pleistocene sea-level fluctuations (Karner and Marra, 1998; Marra et al., 2016a, 2017a), as well as to date several archaeological sites of the Latium region (Marra et al., 2014a, 2015, 2016b, 2017b, 2018; Villa et al., 2016; Petronio et al., 2017, 2019; Ceruleo et al., 2019).

The aggradational successions are defined as the sedimentary packages deposited in response to sea-level rise during the Middle Pleistocene glacial terminations (Marra et al., 2008, 2016a). Usually, they are represented by a fining upward deposit with gravel at the base and abruptly transitioning to a thick clayey section. Specifically, the gravel-clay transition is considered a close proxy of the main melt-water pulse during glacial to interglacial termination. A growing number of $^{40}Ar/^{39}Ar$ ages obtained over the years on volcanic layers interbedded within these sedimentary deposits, demonstrated the agreement between the $\delta^{18}O$ astrocalibrated curve and the independent chronology of the aggradational successions deposited in the delta of the Paleo-Tiber River (Alvarez et al., 1996; Karner and Renne, 1998; Marra et al., 1998, 2016a, 2017a; Florindo et al., 2007; Pereira et al., 2020; Giaccio et al., 2021). Moreover, due to a ~50 m tectonic uplift affecting the Tyrrhenian Sea margin of central Italy since 250 ka (Marra et al., 2016c), elevation at which these successions occur provides further means of correlation. Ten aggradational successions correlating Marine Isotope Stage (MIS) 21 through MIS 1 (Marra et al., 2008) were recognized in

* Corresponding author.
E-mail address: fabrizio.marra@ingv.it (F. Marra).

https://doi.org/10.1016/j.quaint.2021.12.016
Received 25 June 2021; Received in revised form 7 December 2021; Accepted 21 December 2021
Available online 5 January 2022

the coastal area of Rome. These are represented by a series of discontinuous sedimentary deposits ("aggradational sections", Karner and Marra, 1998), for which were given formal formation names (Luberti et al., 2017, and references therein).

In this study, we present the results of extensive dating of geologic sections cropping out west of Rome, along the Via Aurelia (Fig. 1), which was carried out within a broader archaeological research project by Villa et al. (2021). Two well-known Palaeolithic sites of central Italy are located within these sections: Castel di Guido (Radmilli and Boschian, 1996, and references therein) and Malagrotta (Cassoli et al., 1982).

Marra et al. (2018) provided a preliminary correlation of these sites with the MISs. Four $^{40}Ar/^{39}Ar$ ages are in publication by Villa et al. (2021). Here we present an updated geochronological framework outlined by four new samples dated within this study. We use this detailed dataset to constrain the age of sediment aggradation in several geological sections cropping out along the Via Aurelia, i.e. within the inner margin of the Paleo-Tiber delta (Fig. 1). Consequently, we can assess stratigraphy and geometry of the MIS 13 and MIS 11 aggradational successions. Moreover, thanks to the newly acquired geochronologic constraints, we also reconstruct a detailed sea-level history of the MIS 10 - MIS 11 interval, showing that also these near-coastal aggradational sections were very responsive to glacio-eustatic fluctuations. Finally, we also provide very precise age constraints to compare the Relative Sea Level curves and the Oxygen Isotopes records.

2. Geologic setting of the investigated area

The investigated area is located to the west of Rome, in the area inland of the Tiber River mouth (Fig. 1), where the Paleo-Tiber delta was situated between 800 and 600 ka (Marra and Florindo, 2014, and references therein). It is part of the Tyrrhenian Sea margin of central Italy, developed as a back-arc basin since the Miocene. Later, during the Middle-Upper Pleistocene, this sector was affected by continuous, explosive volcanic activity of the high potassic Roman Magmatic Region (Conticelli and Peccerilllo, 1992), including the Monti Sabatini and Colli Albani districts, located respectively W and SE of Rome (Fig. 1). This volcanic activity originated several tephra layers, which are intercalated within the sedimentary successions and provide precise ages by single-crystal, total fusion $^{40}Ar/^{39}Ar$ dating method. Two major uplift pulses at 800 ka and since 250 ka interpunctuated a moderate subsiding regime in the Tiber delta, leading to the progressive seaward shifting of the coast (Marra et al., 2019a, b). Since this period, sedimentary processes in the coastal and in the inland areas were controlled by glacio-eustatic fluctuations (Luberti et al., 2017, and references therein).

3. Material and methods

3.1. $^{40}Ar/^{39}Ar$ dating

The samples dated within this study, as well as those analyzed in Villa et al. (2021), were analyzed at the Laboratoire des Sciences du Climat et de l'Environnement (CNRS-CEA, Gif-sur-Yvette), France, using the procedures described in detail in Pereira et al. (2020). Single crystal measurements were carried out on potassic feldspars, 500-250 μm in size. Ages were calculated according to the K total decay constant of Renne et al. (2011) and the monitor flux standard ACs-2 dated to 1.1891 Ma (Niespolo et al., 2017). Procedural blanks were measured every two or three unknown samples. Mass discrimination was monitored by analysis of air pipette throughout the analytical period, and relative to a $^{40}Ar/^{36}Ar$ ratio of 298.56 (Lee et al., 2006). Results for each dated sample are presented as probability diagrams Fig. 2; full analytical data are provided in Supplementary Material #1.

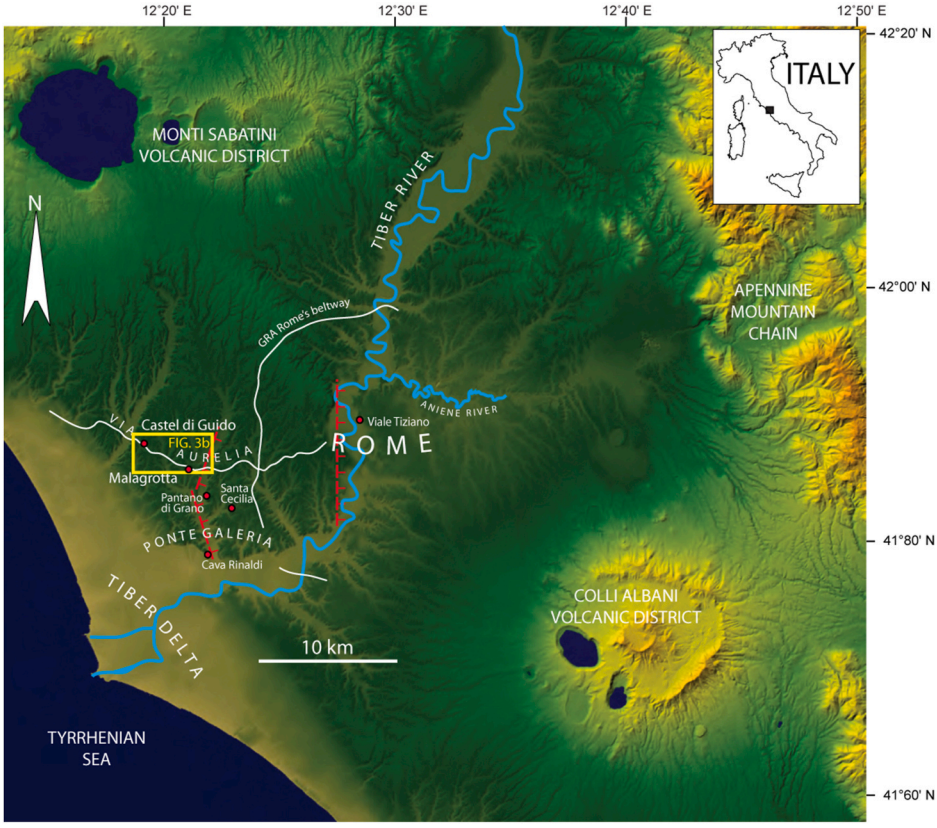

Fig. 1. Study area showing location of the investigated sites and position of inferred faults (red lines). Digital Elevation Map in inset: TINITALY/01 square WA 6570, property of the Istituto Nazionale di Geofisica e Vulcanologia, Rome, http://tinitaly.pi.ingv.it/, used under permission. (For interpretation of the references to colour in this figure legend, the reader is referred to the Web version of this article.)

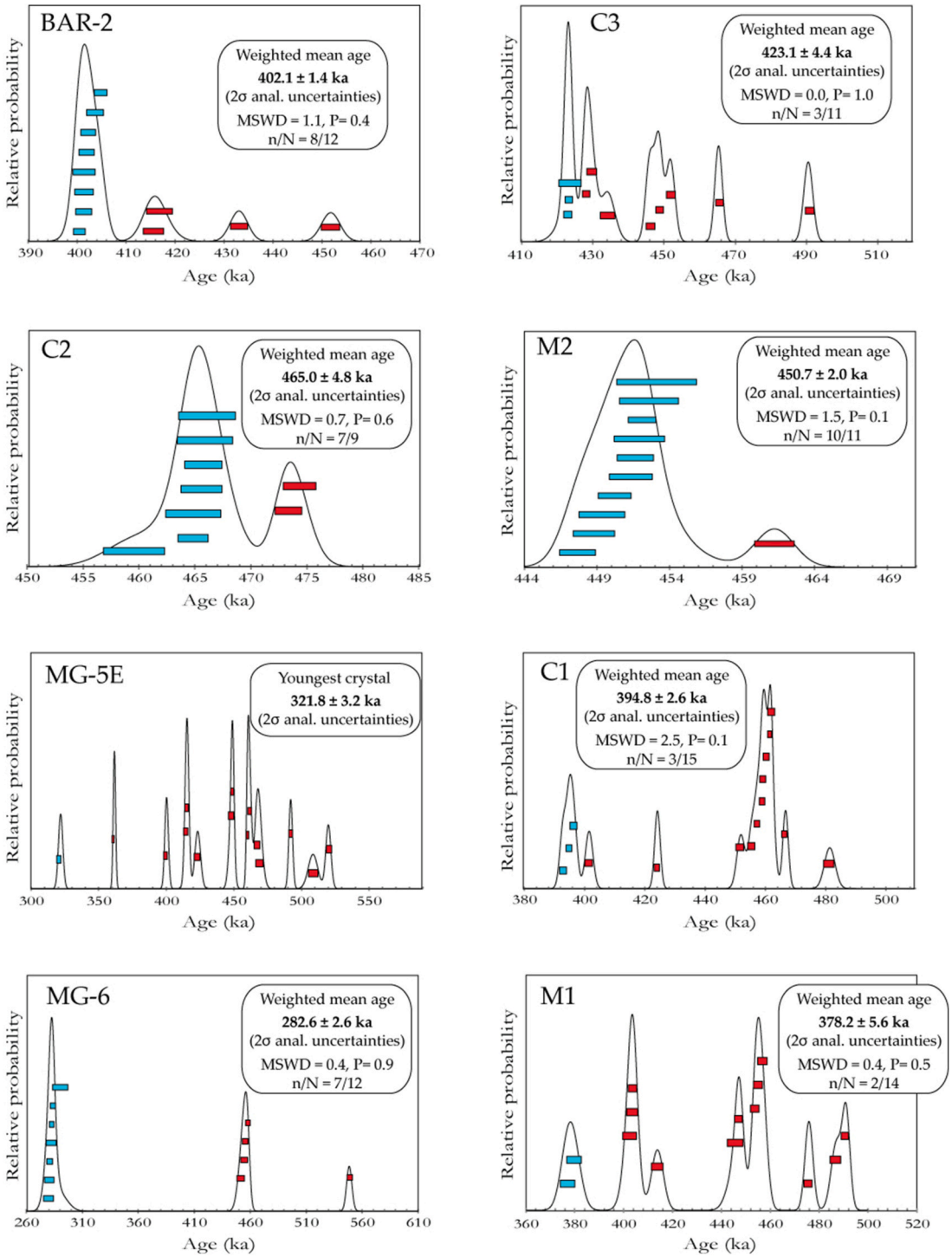

Fig. 2. $-^{40}Ar/^{39}Ar$ results as probability diagrams. Individual crystal error bars are reported at 1σ. For each dated sample, the age reported corresponds to the weighted mean age of the youngest crystal(s) (reported in blue). All ages in the text are reported with 2σ uncertainty. Ages from literature are re-calculated, when appropriate, according to the calibration at 1.1891 Ma for the ACs standard adopted in this paper. (For interpretation of the references to colour in this figure legend, the reader is referred to the Web version of this article.)

4. Results

4.1. $^{40}Ar/^{39}Ar$ dating

Results for each dated sample are presented as probability diagrams (Fig. 2); full analytical data and detailed results are provided in Supplementary Material #1.

The probability diagrams provided for BAR-2, C2, M2 and MG-6 show a main mode computed on at least 7 juvenile crystals. Crystal populations for these samples fulfill statistic fits (Probability (P) > 0.1; Mean Square Weighted Deviation (MSWD) < 2), suggesting that the dated volcanic material is primary or sub-primary and that a robust age of the eruption can be assessed. We calculated the following weighted mean ages for these samples: BAR-2 = 402.1 ± 1.4 ka; C2 = 465.0 ± 4.8 ka; M2 = 450.7 ± 2.0 ka; MG-6 = 282.6 ± 2.6 ka (ages are given at 2σ including J uncertainty). For all these samples, the $^{40}Ar/^{36}Ar$ initial

ratios calculated from the inverse isochrones are compatible with the atmospheric composition ($^{40}Ar/^{36}Ar \sim 298.56$, Lee et al., 2006).

The probability diagrams of the other dated samples are much more complex, corresponding to clearly reworked volcanic units. In these cases, we assume that the youngest crystal population is the maximum age of the sediment deposition (see Marra et al., 2019a for a discussion about the confidence of this approach in providing reliable age constraints). Weighted mean ages calculated for these youngest populations are the following: M1 = 378.2 ± 5.6 ka (calculated on 2 out of 14 dated crystals: n/N = 2/14); C3 = 423.1 ± 4.4 ka (n/N = 3/11); C1 = 394.8 ± 2.6 ka (n/N = 3/15); MG-5E = 321.8 ± 3.2 ka (n/N = 1/15).

Elevation of the dated samples was measured by a portable GPS and is provided with ±1 m accuracy throughout the text.

4.2. New chronostratigraphic reconstruction

The age constraints provided by three of the samples dated in this study (C-3, BAR-2, M2) allowed us to recognize three aggradational sections along the Via Aurelia between Castel di Guido and Malagrotta (outcrops A, B, C, in Fig. 3a), all belonging to the same aggradational succession, known as San Paolo Formation (Karner and Marra, 1998). These outcrops were previously attributed to the Valle Giulia Formation (MIS 13), by correlating the pyroclastic-flow deposit occurring at the base of the exposed sedimentary successions with Tufo Giallo di Prima Porta (TGPP, 516.9 ± 1.3 ka, Marra et al., 2017a) (Marra et al., 2018). In contrast, the samples dated in this study provided younger ages, ranging within 451- 378 ka and demonstrating that these sections expose rather a MIS 12/MIS 11 succession.

The Valle Giulia Formation is exposed between 54 and 58 m a.s.l. at the NW margin of the investigated area, where a primary fallout layer dated at 514.3 ± 4.0 ka (CDG-1, Marra et al., 2018) provides straightforward correlation with MIS 13 (Fig. 3a). Moreover, fluvial/lacustrine deposits occurring between 63 and 60 m a.s.l. underneath the Castel di Guido archaeological layers are geochronologically constrained here within MIS 13, based on the $^{40}Ar/^{39}Ar$ age of 465.0 ± 4.8 ka yielded by sample C2 dated in the present study. These two outcrops occur at elevations remarkably higher than the 40 m a.s.l. estimated for the top of the MIS 13 aggradational succession in the original coastal sector (Cava Rinaldi site, Marra et al., 2017a; see Fig. 1).

In contrast, at the three aggradational sections A, B and C (Fig. 3a), the top surface of San Paolo Formation occurs only at slightly higher elevation (~60 m a.s.l. blue dashed line in Fig. 3a) than the top surface in the equivalent coastal sector (56 m a.s.l., Santa Cecilia site, Pereira et al., 2020). The base of the MIS 11 sedimentary deposits is exposed at 46 m a.s.l. in Malagrotta, on the eastern flank of the Casale Bruciato hill ridge (Figs. 3b and 4b), where they overlie a pyroclastic-flow deposit (M2) dated at 450.7 ± 2.0 ka. The homogeneous crystal population of this pyroclastic flow (Fig. 2) evidences that it is sub-primary, and suggests its correlation with the Tufo Rosso a Scorie Nere eruption unit (TRSN, 453.4 ± 2.0 ka, Marra et al., 2014b). The pyroclastic-flow deposit overlies a markedly erosive surface above the sandy gravel deposits of the Santa Cecilia Formation (649–600 ka, Marra and Florindo, 2014). The top of the sedimentary succession at this section is not exposed, but it can be assessed based on the occurrence of a ~3 m-thick volcaniclastic horizon, including mm-sized dark grey scoriae and loose crystals, occurring 62–65 m a.s.l. at km 16.6 of Via Aurelia, where it overlies the TRSN primary deposit. One sample of this volcaniclastic deposit yielded a youngest crystal population age of 381.8 ± 2.1 ka (sample MG4 in Fig. 3a) (Petronio et al., 2019) allowing us to provide a maximum elevation of ca. 62 m for the top of the MIS 11 deposits (Fig. 3a).

The inferred elevation of the San Paolo Formation top surface at Malagrotta is supported by the new geochronologic constraint to the aggradational section B, located at km 19.3 of Via Aurelia. Sample BAR-2 collected at 57 m a.s.l. in the volcanic deposit previously attributed to the TGPP yielded crystal ages ranging 453–400 ka, with a youngest population of 402.1 ± 1.4 ka (Fig. 2). It is therefore a reworked deposit, emplaced during the late stages of MIS 11 sea-level rise, consistently with its position within the uppermost part of the aggradational

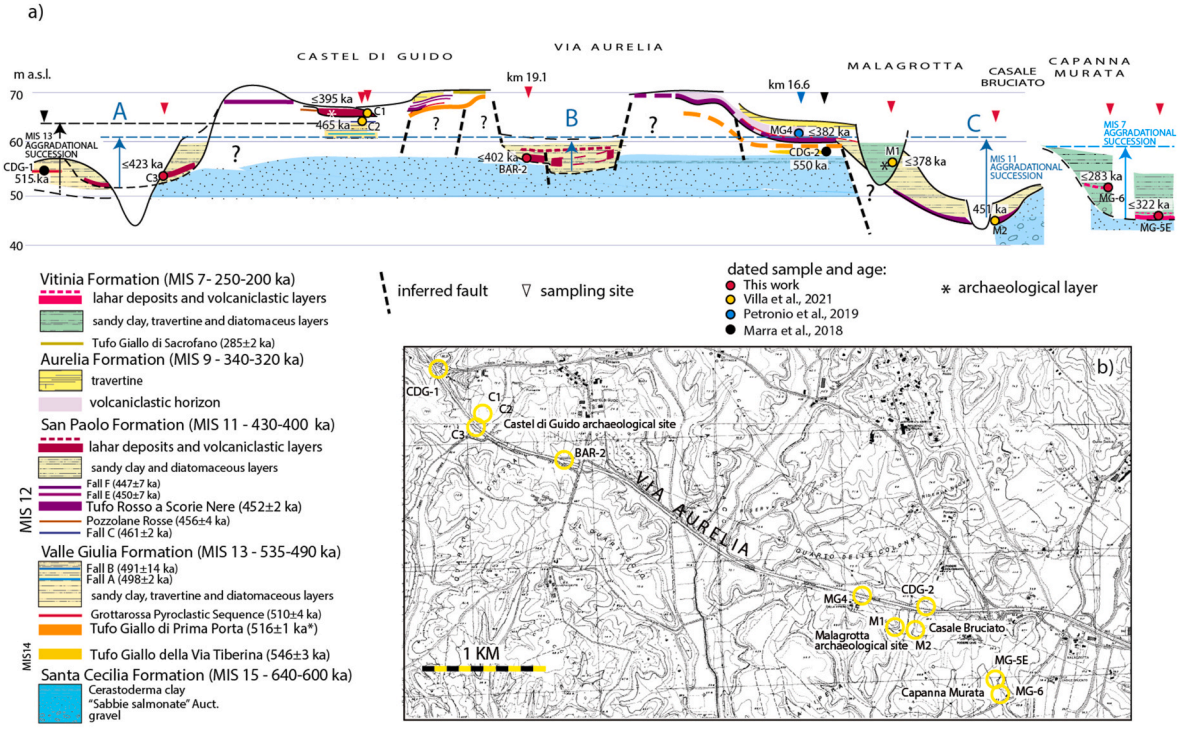

Fig. 3. Composite cross-section showing the schematic stratigraphy of the investigated sites (for the detailed stratigraphic logs see Marra et al., 2018). Stratigraphic position of the archaeological layers of Castel di Guido and Malagrotta is also shown. b) Sampling site locations; topographic map: Carta tecnica regionale 10K formato TIFF, 1990–91, Regione Lazio, available under the Creative Commons Attribution license at: http://dati.lazio.it/weblist/cartografia/prodotti/1990_1991_CTR_10K_TIF/).

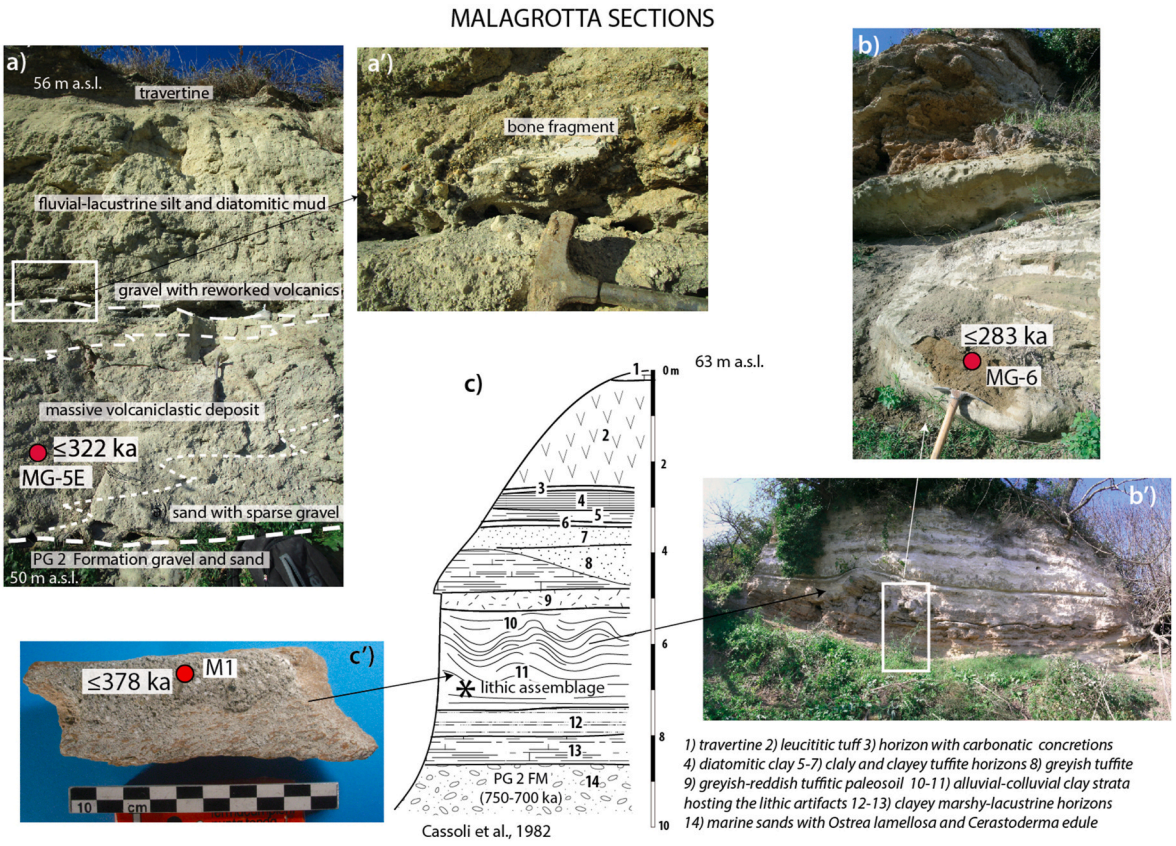

Fig. 4. The two outcrops exposing the MIS 7 aggradational successions investigated in this work (see Fig. 3b for location) are compared with the stratigraphic sketch of the Malagrotta archaeological section redrawn here for illustrative purpose after description in Cassoli et al. (1982). Location of samples dated in this work and in Villa et al. (2021) is also shown. See text for comments. Photos by Giovanni Boschian and Fabrizio Marra.

succession. Sample C3, collected at 53 m a.s.l. close to Castel di Guido (section A in Fig. 3a), yielded scattered crystal ages with a youngest population of 423.1 ± 4.4 ka (Fig. 2), consistent with the occurrence of this volcaniclastic horizon at intermediate elevation within the MIS 11 aggradational succession San Paolo Formation (Fig. 3a).

The outlined framework for the MIS 11 aggradational succession finds further support from the chronostratigraphic data achieved at Castel di Guido. Here, the homogeneous age of 465.0 ± 4.8 ka yielded by sample C2 collected in a pyroclastic layer ca. 1 m below the archaeological horizon, combined with the youngest crystal age of 394.8 ± 2.6 ka yielded by sample C1 collected in the volcaniclastic deposit sealing the archaeological horizon, confirms the lack of MIS 11 aggradational deposits above 60 m a.s.l. (Fig. 3a). Moreover, it allows to interpret the artifact-bearing gully-like paleosurface (Boschian and Saccà, 2010) as an incipient erosional feature developed during the early stages of the regressive phase following MIS 11 highstand (400 through 395 ka).

Maximum ages of 321.8 ± 3.2 and 282.6 ± 2.6 ka yielded by samples MG-5E and MG-6 respectively, highlight that deposits of the younger MIS 7 aggradational succession crop out in the Fosso Galeria valley, at the eastern end of the investigated area (Figs. 1–3b). Similarly, deposits of the Vitinia Formation type-section crop out in the nearby Pantano di Grano, where $^{40}Ar/^{39}Ar$ constraints indicate ages of 268 - 248 ka (Marra et al., 2016a).

Finally, we ascribe to the MIS 7 aggradational succession also the currently re-buried archaeological section of Malagrotta, based on the following considerations.

The exact location of the Malagrotta archaeological section and its identification with a presently visible outcrop is problematic due to incomplete and sometimes conflicting information provided in literature (see Ceruleo et al., 2019 for a discussion). Through a dedicate archive research we have now rescued original documentation that allowed us to unambiguously locate the Malagrotta section on a hillside (Fig. 3b) which is totally covered by debris and overgrown with vegetation. Moreover, such documentation also indicates precisely the location of the bone fragment dated in Villa et al. (2021) within the archaeological horizon excavated at Malagrotta, which yielded an Acheulean lithic assemblage similar to the CDG one (Anzidei and Sebastiani, 1984; Anzidei et al., 1993; Radmilli and Boschian, 1996; Villa et al., 2021).

Pyroclastic material adhering to this bone fragment (sample M1) yielded a weighted mean age of 378.2 ± 5.6 ka, remarkably similar to a sample (MG4) collected in a volcaniclastic layer cropping out at Via Aurelia km 16.4, dated at 381.8 ± 2.1 ka (Petronio et al., 2019). However, the stratigraphic position of this bone fragment, within a suite of silty lacustrine sediments with convoluted features occurring ca. 56 m a.s.l. (Fig. 4c), at lower elevation than the top of the MIS 11 aggradational succession, clearly indicates that this is a reworked inclusion and its age should be regarded as a *terminus post-quem* (minimum age) for the time of deposition of the lacustrine succession. Moreover, we have found the following striking similarities between the stratigraphic sketch of Malagrotta published by Cassoli et al. (1982) and the two outcrops of the MIS 7 aggradational succession at Capanna Murata and nearby site (Fig. 3). An idiosyncratic wavy horizon occurs at Malagrotta and Capanna Murata (Figure ab-b'); at the nearby outcrop, a volcaniclastic layers yields bone fragments with adhering pyroclastic material (Fig. 4a-a') that is quite identical to the Malagrotta one. Finally, abundant intercalations of reworked, older volcaniclastic materials occur also in these sections, like in the type section of the MIS 7 aggradational succession at Pantano di Grano (Marra et al., 2016a).

5. Discussion

5.1. Constraints to sea-level oscillations

The new geochronologic constraints achieved by this study integrate those recently provided by Pereira et al. (2020) and Giaccio et al. (2021) for the San Paolo Formation sediment aggradation on the coast west of Rome. These data can be used in constraining sea-level change in the time span encompassing the MIS 12 early deglaciation phase and the MIS 11 early climatic cooling.

Fig. 5a shows the coincidence between the early aggradation phase preceding the Glacial Termination (GT) V and the sea-level oscillation occurred 450 through 440 ka evidenced on the Relative Sea Level (RSL) curve by Grant et al. (2014). The new data from the aggradational sections of Via Aurelia provide further evidence of this temporary sea-level rise occurred at the end of MIS 12 lowstand and allow to better constrain its age boundaries. We stress the paleoclimatic significance of the TRSN pyroclastic-flow deposit lying on an erosional surface cropping out near the bottom of a stream valley at Malagrotta (Fig. 5b). The limited erosion of the primary volcanic deposit suggests that it emplaced at the end of the erosional phase associated with MIS 12 lowstand. Subsequently, it was preserved because the incipient sea-level rise and consequent sediment aggradation caused its early coverage. Therefore, the age of 450.7 ± 2.0 ka yielded by sample M2 provides a close time constraint to the end of MIS 12 lowstand and to the onset of the deglaciation phase leading to GT V.

Pereira et al. (2020) also showed that the previously estimated age of 423.5 ± 5 ka (sample C3) for the start of GT V should be discarded because the dated sample was contaminated by xenocrystals. Therefore, GT V was bracketed between 438.7 ± 1.2 and 414.8 ± 2.4 ka (Fig. 5a). The lahar at the base of the aggradational section at site C3 provides a new, intermediate age constraint because its age of 423.1 ± 4.4 ka can be regarded as a close *terminus ante-quem* (minimum age) for the rapid sediment aggradation during MIS 11 sea-level rise. Consequently, it provides the best independent age constraint for GT V, so far: >423.1 ± 4.4 <438.7 ± 1.2 ka.

Inferences about the occurrence of a rapid aggradational phase and on its completion time are confirmed by another lahar deposit cropping out within the San Paolo Formation, close to the top of the aggradational section at km 19.1 of Via Aurelia (sample BAR-2), which yielded a youngest crystal population of 402.1 ± 1.4 ka. Remarkably, an erosional surface cuts the fluvial-lacustrine deposits of this formation immediately above the dated lahar at this section. Above this erosional surface, cross-bedded volcaniclastics comprising dark grey scoriae and loose crystals are intercalated with the sediments. Similar volcaniclastic deposits occur around 62 m a.s.l. at km 16.4 of Via Aurelia (Petronio et al., 2019). Moreover, the maximum age of the erosional surface occurring at the archaeological site of Castel di Guido is 394.8 ± 2.6 ka, as indicated by sample C1, collected from the overlying lahar deposit. This widespread suite of volcaniclastic deposits unconformably overlying the MIS 11 aggradational succession highlights the onset -by ~380 ka-of the regressive phase following the highstand. These ages provide a robust upper age boundary to the duration of MIS 11 highstand (Fig. 5a).

5.2. Inferences on the amplitude of sea-level oscillations

Based on the geochronologic and stratigraphic data described above, we have reconstructed the geometry of the aggradational sections of MIS 11, MIS 13 and MIS 7 in this area and we have compared their top surfaces and thickness with those assessed in previous studies in the coastal area of Ponte Galeria (Santa Cecilia-Pantano di Grano, MIS 11 and MIS 7) and in the Tiber River channel (Viale Tiziano, MIS 13) (Fig. 6a).

The top surfaces of these three sedimentary packages along Via Aurelia occur at similar, slightly decreasing elevation as a function of their age: the older the higher. The MIS 13 aggradational succession (herby AGS) top surface occurs at much higher elevation (ca. 63 m a.s.l.) than the estimated one for the inland Tiber River channel (ca. 48 m, Marra et al., 2017a, Fig. 6a). This difference may have resulted from ~20 m tectonic drop of the central Rome area lower than the Ponte Galeria area (Marra et al., 2016a), which possibly occurred during MIS 9 (Marra et al., 2019a). Similarly, the slightly lower elevation of the top surface of MIS 11 and MIS 7 AGSs can be explained by ~5 m tectonic lowering east of the Fosso Galeria fault line (see Fig. 1; Marra and Florindo, 2014).

We also observe comparable estimated thicknesses (i.e. ~15 m) for MIS 11 and MIS 7 AGSs along Via Aurelia, which are about 60% of the estimated ones in the coastal area for the equivalent AGSs (~25 m). MIS 13 AGS is also about 15 m thick along Via Aurelia while it is about 30 m thick within the Tiber valley in Viale Tiziano north of Rome. All these differences in thickness are likely due to different base levels in the investigated areas, which depended on the location relative to fluvial channel and coastline (i.e., the gradient of the basal erosional surface). We use the more reliable datum of the AGSs top surfaces as relative sea-level indicators to refine the tectonic vs. glacio-eustatic forcing on sediment aggradation in the coastal area of Rome in Fig. 6b–c, following a well-established approach developed in the last years (e.g., Marra et al., 2019a, and references therein).

According to this methodological approach, we assume that the top surfaces of all these AGSs, affecting coastal to lagoon sediments,

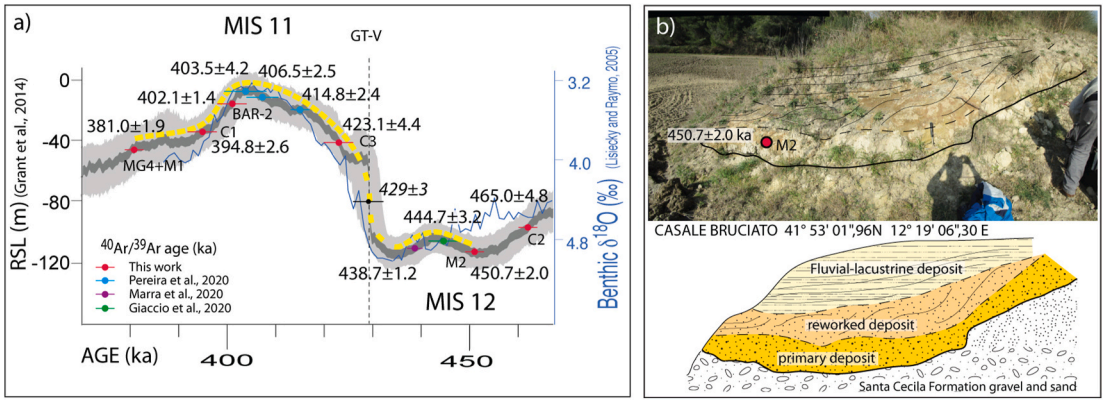

Fig. 5. a) The yellow line represents sediment aggradation vs. time derived from the geochronologically constrained aggradational succession of the San Paolo Formation. Its vertical amplitude is conventionally scaled to compare the sea-level curve and the isotopic signal. The $^{40}Ar/^{39}Ar$ ages (blue and red dots) are plotted on the RSL curve to compare the timing of aggradation with the sea-level fluctuations. b) Outcrop of the primary pyroclastic-flow deposit in which sample M2 was collected (see Fig. 3b for location). Photo by Fabrizio Marra. (For interpretation of the references to colour in this figure legend, the reader is referred to the Web version of this article.)

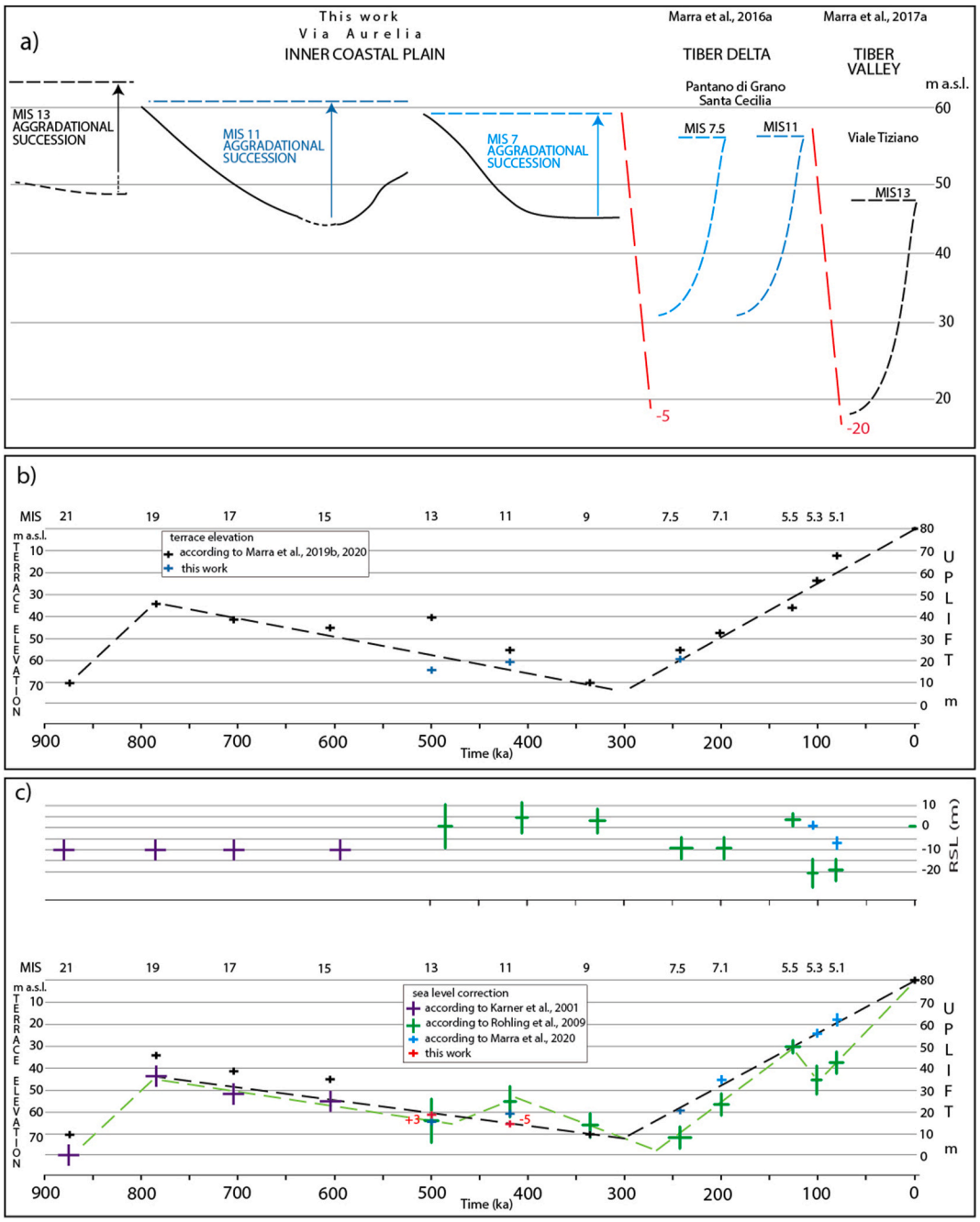

Fig. 6. a) Schematic reconstruction of the geometry of three aggradational successions correlated with MIS 13, MIS 11 and MIS 7 based on the Via Aurelia outcrops, and comparison with their equivalents from the coastal area and from the Tiber Valley. b) Coastal terrace elevations from previous literature and from this study are used as sea-level proxy to reconstruct the tectonic uplift (dashed line) in this region, in the hypothesis that maximum sea level was equal at each interglacial. c) Proposed differences in absolute sea level with respect to the Present for MIS 21 through MIS 15 highstands (Karner et al., 2001), from MIS 13 though MIS 5.1 (Rohling et al., 2009) and for MIS 7.1, 5.5, 5.1 (Marra et al., 2020b) are used for the sea level correction to the uplift curve (see Marra et al., 2019a, 2020b for an in-depth discussion). The green dashed line represents the uplift history based on average sea-level corrections from Karner et al. (2001) and Rohling et al. (2009). The dashed black line represents a steady uplift curve based on sea levels inferred in this work from terrace elevations for MIS 13, MIS 11, and MIS 7.5. We note that a better fit with the rectilinear trend associated with a steady tectonic rate is obtained based on the sea-level proxies proposed here for MIS 13 and MIS 11. Moreover, a sea-level correction of +3 and −5 m with respect to Present-day should be applied to fit the steady tectonic rate, exactly, according to these proxies (red crosses), suggesting a higher absolute sea level during MIS 13 highstand with respect to MIS 11 highstand (see text for discussion). (For interpretation of the references to colour in this figure legend, the reader is referred to the Web version of this article.)

represent remnants of the original coastal plain (i.e., coastal terraces). A corresponding sea level is estimated following their average elevation (black cross in Fig. 6b), with an approximation of 0 to −5 m. The following considerations are purely qualitative, aimed at highlighting general trends, and assume that uncertainties linked with the estimated sea-level elevations do not hinder the regional tectonic trends.

In Fig. 6b, we use the newly determined elevation of 64 m a.s.l. for the MIS 13 terrace, differently from a previous estimate of 40 m at Cava Rinaldi site (Marra et al., 2016c). The previous estimate was evidently based on incomplete preservation (erosion) of the sedimentary package cropping out in this location; moreover, it did not consider the elevation of about 48 m reported for the inland tract of the Tiber Valley (Viale

Tiziano locality) in Marra et al. (2017a). Additionally, we introduce the elevations observed in the tectonically more stable area of Via Aurelia for MIS 11 and MIS 7 terraces (blue crosses in Fig. 6b).

When no noticeable difference in maximum sea level between each highstand and the Present is assumed, the dashed black line in Fig. 6b represents the regional uplift affecting the coastal area during the last 900 ka. As highlighted in previous work (e.g., Marra et al., 2019a, and references therein) two major uplift phases affected this area, one between 900 and 800 ka, and another one between 300 ka and the Present (Fig. 6b). These uplift phases were separated by a steady subsiding regime, coeval with the major phases of explosive activity of the Roman Province volcanic districts in the interval 600–300 ka (Marra et al., 2020a). We note that the elevations introduced here for the MIS 13, 11 and 7 terraces provide a better fit with a supposed steady uplift/subsidence rate (they plot closer to the curve), when considered indicative of sea level during the highstands. Conversely, when sea-level differences between each highstand and the Present available in literature are considered (e.g., Karner et al., 2001; Rohling et al., 2009), several of the introduced corrections result in a larger misfit (sea levels plot at greater distance) with respect to the rectilinear tracts pertaining to a steady tectonic regime (see Marra et al., 2019a for an in-depth discussion of this topic). In fact, it was already suggested in (Marra et al. 2019b, 2020b) that benthic δ^{18}O-derived sea levels for MIS 5.3 and 5.1 (~−20 m) may be underestimated in the Mediterranean region and should be re-assessed at 1/-3 m and −4/-10 m, respectively (light blue crosses in Fig. 5c). Here, we note the same possible underestimate for MIS 7.5 and 7.1 sea levels, while we remark that corrections of ~ +3 and −5 m should be applied to MIS 13 and MIS 11 sea levels respectively, based on terrace elevations along the coast of Rome (red crosses in Fig. 6c).

These sea-level corrections based on terrace elevations combined with steady tectonic rates provide maximum sea-levels at the interglacials spanning MIS 13 thorough MIS 5.1 (Fig. 7b) which differs from those estimated in the literature (e,g., Rohling et al., 2009 and references therein). In particular, data from the aggradational successions of Via Aurelia suggest that sea-level was higher during MIS 13 highstand than during MIS 11, contrasting with global sea levels assessed from δ^{18}O-derived ice volume and speleothems estimations (Rohling et al., 2009). However, if the associated errors are considered (height of the green crosses in Fig. 7c) the MIS 13 and MIS 11 sea levels in Rohling et al. (2009) are still compatible with estimates along the coast of Rome.

Finally, it should be remarked that when comparing the locally observed (or inferred) RSL change to the eustatic process within the Mediterranean Basin the Glacial Isostatic Adjustment (GIA) effect cannot be neglected. The latter results in a regionally-varying signal that depends on the pattern of ice sheets retreat and on the solid Earth rheology (e.g., Stocchi et al., 2018). Indeed, different global ice volumes for different periods might result in similar local RSL curves as a consequence of the way the ice mass is distributed over the continent.

5.3. Age constraints of the archaeological sites

In the following sections we illustrate the paleoclimatic and stratigraphic principles underlying to the assessment of the age of the archaeological materials (both fossils and lithic assemblages) recovered at CDG and MG. We remark that this combined methodology allows to reconstruct the depositional context of the archaeological horizons, providing information on the time of deposition as well as on the depositional process which affected the artifacts, evidencing their primary or reworked features.

5.3.1. Castel di Guido: >381.0 ± 1.9 ka ≤394.8 ± 2.6 ka

The lithic and bone artifacts and the faunal remains recovered at Castel di Guido rested upon an erosional paleosurface sealed by a reworked, matrix-supported volcaniclastic deposit (mudflow) (Boschian and Saccà, 2010; Marra et al., 2018; Ceruleo et al., 2019) (Fig. 8a).

This paleosurface must be older than the maximum age yielded by sample C1, collected in the overlying volcaniclastic deposit (i.e. 394.8 ± 2.6, weighted mean age of the three youngest crystals, Fig. 2). Moreover, we assume an age >381.0 ± 1.9 ka (combined age of the two samples M1 and MG4, Fig. 3) for the emplacement of the mudflow at Castel di Guido, based on the lack of a crystal population of this younger age, which is common in the widespread volcaniclastic horizon cropping out at Via Aurelia km 16.6 and at MG (Fig. 3a). In fact, continued volcanic activity occurred within the Monti Sabatini Volcanic District between 452 and 380 ka (Marra et al., 2020a), and it is reasonable to assume that the age of the youngest crystal population in sample C1 also provides a maximum age for the volcaniclastic deposit. As discussed in Marra et al. (2019a), the youngest eruptions should be better represented in reworked deposits because their products crop out in wider areas than the old ones, which are buried under a longer sequence of strata. This consideration supports the principle that the age of a layer is bracketed between the ages of its youngest crystal population and of the next younger eruption, whose crystals do not occur in the layer but is widely

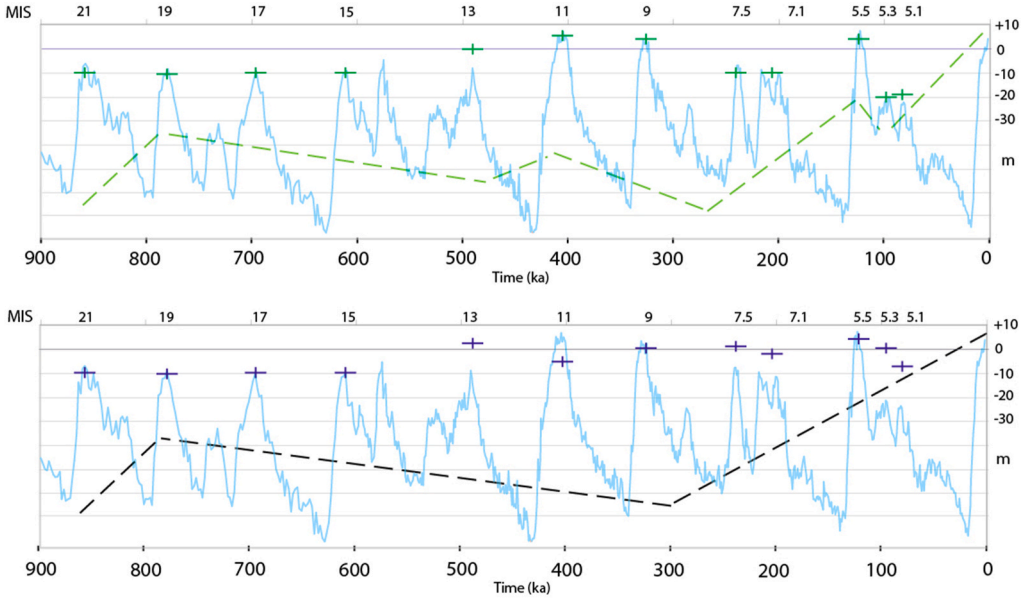

Fig. 7. a) Average maximum sea level (green crosses) at interglacials according to estimations based on δ^{18}O-derived ice volume and speleothems estimations; the dashed green line is the uplift history in the coastal area of Rome reconstructed using these sea-level corrections with respect to Present-day. b) Average maximum sea level (blue crosses) at interglacials according to terrace elevations combined with a steady uplift rate in the coastal area of Rome. δ^{18}O curve by Lisiecki and Raymo (2005). . (For interpretation of the references to colour in this figure legend, the reader is referred to the Web version of this article.)

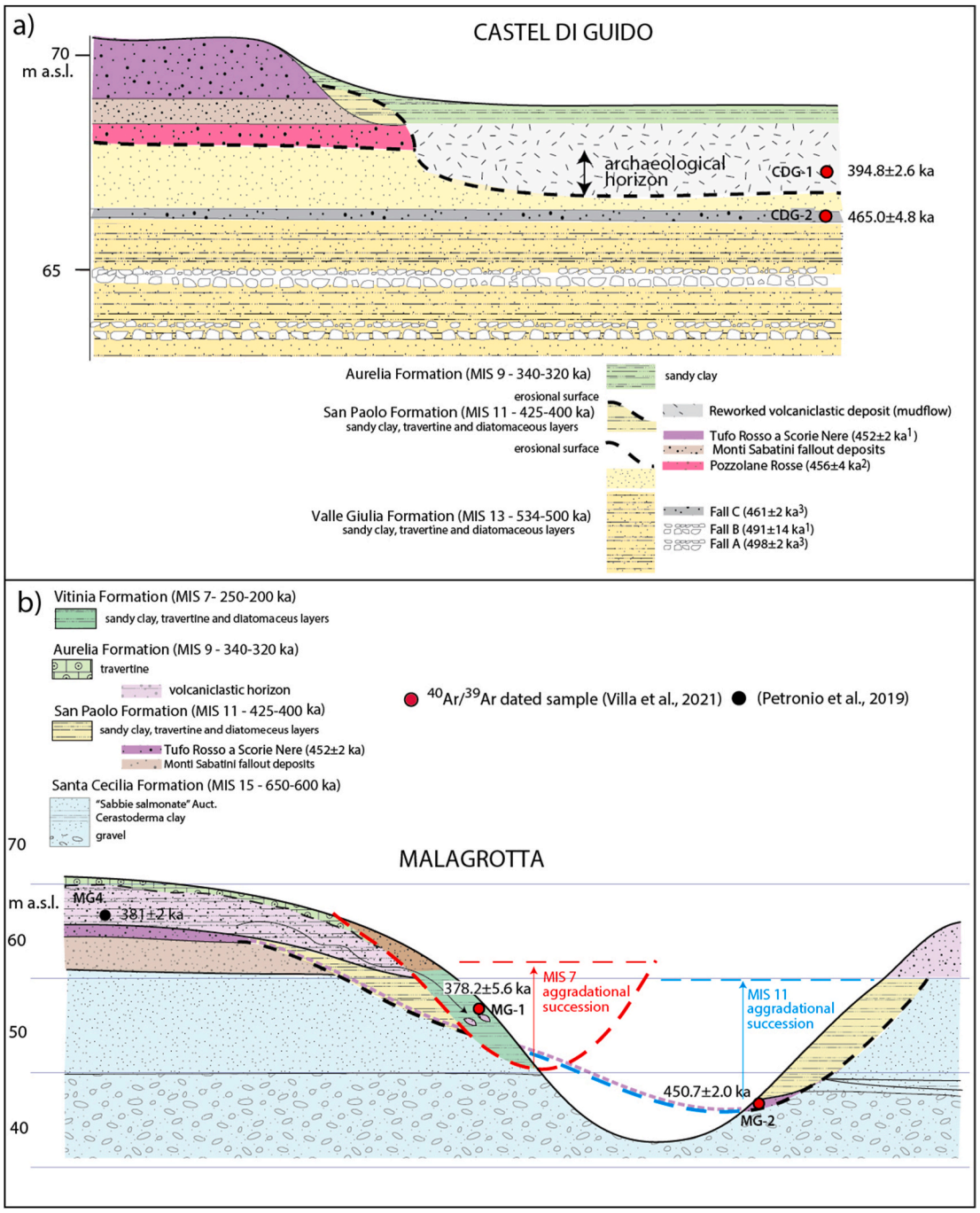

Fig. 8. Stratigraphic sketches of Castel di Guido (a) and Malagrotta (b) archaeological sites. An alternative hypothesis with respect to that reported in Fig. 3 is provided here for the stratigraphy of Malagrotta; see text for explanation. Age of volcanic products by Marra et al. (2014b) (1), Marra et al. (2009) (2), Marra et al. (2017a) (3).

documented in the area.

The age of TRSN (450.7 ± 2.0 ka, Villa et al., 2021), which is eroded by the paleosurface (Fig. 8a), provides a lower chronological boundary for the age of the archaeological horizon. Moreover, we claim that this incipient erosive surface must be younger than the MIS 11 sea-level highstand (403.5 ± 4.2 ka, Pereira et al., 2020) (Fig. 5a), because the following considerations suggest that it originated during the subsequent regressive phase. The lack of any sediment between it and the overlying volcaniclastic deposit suggest both that:

i the paleosurface was an ephemeral feature that was sealed by the sudden deposition of the mudflow at 394.8 ± 2.6 ka;

ii the paleosurface originated during the late stages of MIS 12, re-eroding the TRSN pyroclastic-flow deposit, but was not affected by significant deposition because of its higher elevation above the top of the MIS 11 aggradational succession (i.e., ca. 61 m a.s.l.). Therefore, its age may range the whole interval 450–395 ka.

However, the location within the coastal plain and the very short distance from the other sites affected by sediment aggradation make it unlikely the lack of any type of deposition (either alluvial or aeolian) enduring several ka.

Following all these considerations, we suggest that the maximum age of the volcaniclastic deposit (394.8 ± 2.6 ka) is also the closest

approximation of the underlying paleosurface age.

5.3.2. Malagrotta: sedimentary succession ca. 250 ka, archaeological materials 378.2 ± 5.6 ka

As discussed in section 4.2, stratigraphic position and correlation with nearby outcrops evidence that the dated bone fragment occurring in the archaeological horizon of Malagrotta is a reworked inclusion, and the age of 378.2 ± 5.6 ka provides only a *terminus post-quem* to sediment deposition, suggesting that the archaeological section of Malagrotta is also a MIS 7 aggradational section, like the other MIS 7 sections identified in the present study (Fig. 3). However, provenance and age of the lithic materials of Malagrotta are the same as the bone fragment, and they were part of the same archaeological horizon occurring also at CDG, which was covered and embedded by the post-MIS 11 volcaniclastic deposits of ca. 380 ka, successively eroded and re-sedimented within a paleovalley filled by the MIS 7 aggradational succession (Fig. 8b).

6. Conclusions

The age constraints to the MIS 11 aggradational sections of Via Aurelia integrate the large dataset provided in Pereira et al. (2020) and contribute to reconstructing the so-far best chronologically controlled sea-level curve proxy for the Mediterranean region in the 465–381 ka interval (dashed yellow line in Fig. 5a). This proxy provides a minimum age of 423.1 ± 4.4. ka for glacial termination IV and the onset of MIS 11 highstand, and a maximum age of 402.1 ± 1.4 ka for the end of the highstand. A duration of 21 ± 5.8 ka for this highstand is therefore assessed here.

Although lacking quantitative constraints about the absolute amplitude of the sea-level oscillations, our sea-level curve proxy in the 450–381 ka interval is related to a sedimentary record whose total thickness is determined in this study. This value (~15 m) is comparable with the thickness of the MIS 13 and MIS 7 aggradational successions, which are also reconstructed here. Ruling out differences in sediment availability or sediment compaction, based on the fact that the drainage basin and the eroded terrains do not change significantly in time, it can consequently be inferred that all the corresponding glacio-eustatic cycles had similar amplitude, despite their remarkably different isotopic signal. Moreover, the top surface of MIS 13 aggradational succession is higher than the MIS 11 one, despite evidence of an overall regional subsiding tectonic regime 800 through 300 ka (Marra et al., 2016c, 2019b), so challenging the notion that sea level was higher during MIS 11 highstand (e.g., Rohling et al., 2009). No evidence that MIS 11 sea-level highstand was significantly higher than during MIS 13 and MIS 7.5 highstands can be provided by this study.

We are confident that future studies, based on hydrologic, paleogeographic and sedimentologic analyses, combined with comparative similar data on the other aggradational successions of the Paleo-Tiber delta, as well as with detailed estimation of the local GIA (e.g., Stocchi et al., 2018), may provide useful information to assess the absolute amplitude of the glacio-eustatic signal also during the "Glacial Pleistocene" of the Mediterranean region. This may provide a more constrained comparative dataset for testing the global ice volume models.

Author contributions

FM designed the geologic study, performed the field investigations, and wrote the paper. AP performed the $^{40}Ar/^{39}Ar$ analyses and wrote the paper. GB performed the field investigations, and wrote the paper. SN performed the $^{40}Ar/^{39}Ar$ analyses and wrote the paper.

Data availability

$^{40}Ar/^{39}Ar$ full analytical data are available in Supplementary Data File #1.

Funding

This research received no funding.

Declaration of competing interest

☐ X The authors declare that they have no known competing financial interests or personal relationships that could have appeared to influence the work reported in this paper.

Appendix A. Supplementary data

Supplementary data to this article can be found online at https://doi.org/10.1016/j.quaint.2021.12.016.

References

Alvarez, W., Ammerman, A.J., Renne, P.R., Karner, D.B., Terrenato, N., Montanari, A., 1996. Quaternary fluvial-volcanic stratigraphy and geochronology of the capitoline hill in Rome. Geology 24 (8), 751–754.

Anzidei, A.P., Sebastiani, R., 1984. Saggi di scavi nel deposito pleistocenico al km 19,300 della via Aurelia (Castel di Guido). Preistoria e Protostoria nel territorio di Roma, pp. 86–95.

Anzidei, A.P., Caloi, L., Giacopini, L., Mantero, D., Palombo, M.R., Sebastiani, R., Segre, A.G., 1993. Saggi di scavo nei depositi pleistocenici del km. 18,900 della via Aurelia e di Collina Barbattini (Castel di Guido-Roma). Archeologia Laziale 11, 81–90.

Boschian, G., Saccà, D., 2010. Ambiguities in human and elephant interactions? Stories of bones, sand and water from Castel di Guido (Italy). Quat. Int. 214, 3–16.

Cassoli, P.F., De Giuli, C., Radmilli, A.M., Segre, A.G., 1982. Giacimento del Paleolitico inferiore a Malagrotta (Roma). Atti della XXIII Riunione Scientifica dell'Istituto Italiano di Preistoria e Protostoria, Il paleolitico inferiore in Italia, Firenze 7-9 maggio 1980. Istituto Italiano di Preistoria e Protostoria, Firenze, pp. 531–549.

Ceruleo, P., Rolfo, M., Marra, F., Petronio, C., Salari, L., Gatta, M., 2019. New chronologic framework (MIS 13-9) and taphonomical context for the lower Palaeolithic sites north-west of Rome: archaeological evidence for an early human presence in central Italy. Quat. Int. 510, 119–132. https://doi.org/10.1016/j.quaint.2019.01.001.

Conticelli, S., Peccerilllo, A., 1992. Petrology and geochemistry of potassic and ultrapotassic volcanism in central Italy: petrogenesis and inferences on the evolution of the mantle sources. Lithos 28, 221–240.

Florindo, F., Karner, D.B., Marra, F., Renne, P.R., Roberts, A.P., Weaver, R., 2007. Radioisotopic age constraints for glacial terminations IX and VII from aggradational sections of the Tiber River delta in Rome, Italy. EPSL 256, 61–80, 2007.

Giaccio, B., Marino, G., Marra, F., Monaco, L., Pereira, A., Zanchetta, G., Gaeta, M., Leicher, N., Nomade, S., Palladino, D.M., Sottili, G., Guillou, H., Scao, V., 2021. Tephrochronological constraints on the timing and nature of sea-level change prior to and during glacial termination V. Quat. Sci. Rev. 263, 1–15. https://doi.org/10.1016/j.quascirev.2021.106976.

Grant, K.M., Rohling, E.J., Ramsey, C.B., Cheng, H., Edwards, R.L., Florindo, F., Heslop, D., Marra, F., Roberts, A.P., Tamisiea, M.E., Williams, F., 2014. Sea-level variability over five glacial cycles. Nat. Commun. 5 https://doi.org/10.1038/ncomms6076.

Karner, D.B., Marra, F., 1998. Correlation of fluviodeltaic aggradational sections with 1 glacial climate history: a revision of the classical Pleistocene stratigraphy of Rome. Geol. Soc. Am. Bull. 110, 748–758.

Karner, D.B., Renne, P.R., 1998. $^{40}Ar/^{39}Ar$ geochronology of Roman volcanic province tephra in the Tiber River valley: age calibration of middle Pleistocene sea-level changes. Geol. Soc. Am. Bull. 110, 740–747.

Karner, D.B., Marra, F., Florindo, F., Boschi, E., 2001. Pulsed uplift estimated from terrace elevations in the coast of Rome: evidence for a new phase of volcanic activity? Earth Planet Sci. Lett. 188, 135–148.

Lee, J.Y., Marti, K., Severinghaus, J.P., Kawamura, K., Hee–Soo, Y., Lee, J.B., Kim, J.S., 2006. A redetermination of the isotopic abundances of atmospheric Ar. Geochem. Cosmochim. Acta 70, 4507–4512. https://doi.org/10.1016/j.gca.2006.06.1563.

Lisiecki, L.E., Raymo, M.E., 2005. A Pliocene-Pleistocene stack of 57 globally distributed benthic ^{18}O records. Paleoceanography 20, PA1003. https://doi.org/10.1029/2004PA001071.

Luberti, G.M., Marra, F., Florindo, F., 2017. A review of the stratigraphy of Rome (Italy) according to geochronologically and paleomagnetically constrained aggradational successions, glacio-eustatic forcing and volcano-tectonic processes. Quat. Int. 438, 40–67. https://doi.org/10.1016/j.quaint.2017.01.044.

Marra, F., Florindo, F., 2014. The subsurface geology of Rome: sedimentary processes, sea-level changes and astronomical forcing. Earth Sci. Rev. 136, 1–20. https://doi.org/10.1016/j.earscirev.2014.05.001.

Marra, F., Florindo, F., Karner, D.B., 1998. Paleomagnetism and geochronology of early Middle Pleistocene depositional sequences near Rome: comparison with the deep sea ^{18}O climate record. Earth Planet Sci. Lett. 159, 147–164.

Marra, F., Florindo, F., Boschi, E., 2008. The history of glacial terminations from the Tiber River (Rome): insights to glacial forcing mechanisms. Paleoceanography 23, PA2205. https://doi.org/10.1029/2007PA001543.

Marra, F., Pandolfi, L., Petronio, C., Di Stefano, G., Gaeta, M., Salari, L., 2014a. Reassessing the sedimentary deposits and vertebrate assemblages from Ponte Galeria area (Rome, central Italy): an archive for the Middle Pleistocene faunas of Europe. Earth Sci. Rev. 139, 104–122.

Marra, F., Sottili, G., Gaeta, M., Giaccio, B., Jicha, B., Masotta, M., Palladino, D.M., Deocampo, D., 2014b. Major explosive activity in the Sabatini Volcanic District (central Italy) over the 800-390 ka interval: geochronological - geochemical overview and tephrostratigraphic implications. Quat. Sci. Rev. 94, 74–101. https://doi.org/10.1016/j.quascirev.2014.04.010.

Marra, F., Ceruleo, P., Jicha, B., Pandolfi, L., Petronio Salari, L., 2015. A new age within MIS 7 for the *Homo neanderthalensis* of Saccopastore in the glacio-eustatically forced sedimentary successions of the Aniene River Valley, Rome. Quat. Sci. Rev. 129, 260–274. https://doi.org/10.1016/j.quascirev.2015.10.027.

Marra, F., Rohling, E.J., Florindo, F., Jicha, B., Nomade, S., Pereira, A., Renne, P.R., 2016a. Independent $^{40}Ar/^{39}Ar$ and 14C age constraints on the last five glacial terminations from the aggradational successions of the Tiber River, Rome (Italy). Earth Planet Sci. Lett. 449, 105–117. https://doi.org/10.1016/j.epsl.2016.05.037.

Marra, F., Ceruleo, P., Jichac, B., Pandolfi, L., Petronio, C., Salari, L., Giaccio, B., Sottili, G., 2016b. Glacio-eustatic and tectonic forcing on the lacustrine succession of the Cretone basin: chronostratigraphic constraints to Acheulian industry and Middle Pleistocene faunal assemblages of Latium (central Italy). J. Quat. Sci. 31, 641–658.

Marra, F., Florindo, F., Anzidei, M., Sepe, V., 2016c. Paleo-surfaces of glacio-eustatically forced aggradational successions in the coastal area of Rome: assessing interplay between tectonics and sea-level during the last ten interglacials. Quat. Sci. Rev. 148, 85–100. https://doi.org/10.1016/j.quascirev.2016.07.003.

Marra, F., Florindo, F., Jicha, B., 2017a. $^{40}Ar/^{39}Ar$ dating of glacial termination VI: constraints on the duration of marine isotopic stage 13. Sci. Rep. 7, 8908. https://doi.org/10.1038/s41598-017-08614-6.

Marra, F., Ceruleo, P., Pandolfi, L., Petronio, C., Rolfo, M.F., Salari, L., 2017b. The aggradational successions of the aniene river valley in Rome: age constraints to early Neanderthal presence in Europe. PLoS One 12 (1), e0170434. https://doi.org/10.1371/journal.pone.0170434.

Marra, F., Karner, D.B., Freda, C., Gaeta, M., Renne, P.R., 2009. Large mafic eruptions at the Alban Hills Volcanic District (Central Italy): chronostratigraphy, petrography and eruptive behavior. J. Volc. Geoth. Res. 179, 217–232. https://doi.org/10.1016/j.jvolgeores.2008.11.009.

Marra, F., Nomade, S., Pereira, A., Petronio, P., Salari, L., Sottili, G., Bahain, J.-J., Boschian, G., Di Stefano, G., Falguères, C., Florindo, F., Gaeta, M., Giaccio, B., Masotta, M., 2018. A review of the geologic sections and the faunal assemblages of Aurelian Mammal Age of Latium (Italy) in the light of a new chronostratigraphic framework. Quat. Sci. Rev. 181, 173–199. https://doi.org/10.1016/j.quascirev.2017.12.007.

Marra, F., Gaeta, M., Jicha, B.R., Nicosia, C., Tolomei, C., Ceruleo, P., Florindo, F., Gatta, M., La Rosa, M., Rolfo, M.F., 2019a. MIS 9 to MIS 5 terraces along the Tyrrhenian Sea coast of Latium (central Italy): assessing interplay between sea-level oscillations and tectonic movements. Geomorphology. https://doi.org/10.1016/j.geomorph.2019.106843.

Marra, F., Bahain, J.-J., Jicha, B., Nomade, S., Palladino, D.M., Pereira, A., Tolomei, C., Voinchet, P., Anzidei, M., Aureli, D., Ceruleo, P., Falguères, C., Florindo, F., Gatta, M., Ghaleb, B., La Rosa, M., Peretto, C., Petronio, C., Rocca, R., Rolfo, M.F., Salari, L., Smedile, A., Tombret, O., 2019b. Reconstruction of the MIS 5.5, 5.3 and 5.1 coastal terraces in Latium (central Italy): a re-evaluation of the sea-level history in the Mediterranean sea during the last interglacial. Quat. Int. 525, 54–77. https://doi.org/10.1016/j.quaint.2019.09.001.

Marra, F., Castellano, C., Cucci, L., Florindo, F., Gaeta, M., Jicha, B., Palladino, D.M., Sottili, G., Tertulliani, A., Tolomei, C., 2020a. Monti Sabatini and Colli Albani: the dormant twin volcanoes at the gates of Rome. Sci. Rep. 10, 8666. https://doi.org/10.1038/s41598-020-65394-2.

Marra, F., Rolfo, F.M., Gaeta, M., Florindo, F., 2020b. Anomalous last interglacial Tyrrhenian Sea levels and Neanderthal settling at Guattari and Moscerini caves (central Italy). Sci. Rep. 10, 11929. https://doi.org/10.1038/s41598-020-68604-z.

Niespolo, E.M., Rutte, D., Deino, A., Renne, P.R., 2017. Intercalibration and Age of the Alder Creek Sanidine 40Ar/39Ar Standard. Quaternary Geochronology in press. https://doi.org/10.1016/j.quageo.2016.09.004.

Pereira, A., Monaco, L., Marra, F., Nomade, S., Gaeta, M., Leicher, N., Palladino, D.M., Sottili, G., Guillou, H., Scao, V., Giaccio, B., 2020. Tephrochronology of the central Mediterranean glacial Termination V and MIS 11c (~445-395 ka): new constraints from Vico volcano and Tiber valley, Central Italy. Quat. Sci. Rev. 243 https://doi.org/10.1016/j.quascirev.2020.106470.

Petronio, C., Ceruleo, P., Marra, F., Pandolfi, L., Rolfo, M.F., Salari, L., Sottili, G., 2017. A novel multidisciplinary bio- and geo-chronological approach for age determination of Palaeolithic bone artifacts in volcanic settings: an example from eastern Sabatini, Latium, Italy. Quat. Int. 438, 81–89. https://doi.org/10.1016/j.quaint.2017.02.010.

Petronio, C., Di Stefano, G., Kotsakis, T., Salari, L., Marra, F., Jicha, B., 2019. Biochronological framework for the late Galerian and early-middle aurelian Mammal ages of peninsular Italy. Geobios. https://doi.org/10.1016/j.geobios.2019.02.002, 52/2.

Radmilli, A.M., Boschian, G., 1996. Gli scavi a Castel di Guido. Il più antico giacimento di cacciatori nell'Agro Romano. ETS, Pisa.

Renne, P.R., Mundil, L.R., Balco, G., Min, K., et Ludwig, K.R., 2011. Joint determination of 40K decay constants and 40Ar*/40K for the Fish Canyon sanidine standard, and improved accuracy for 40Ar/39Ar geochronology. Response to the comment by W. H. Schwarz et al. Geochem. Cosmochim. Acta 75, 5097–5100.

Rohling, E.J., Grant, K., Bolshaw, M., Roberts, A.P., Siddall, M., Hemleben, Ch, Kucera, M., 2009. Antarctic temperature and global sea level closely coupled over the past five glacial cycles. Nat. Geosci. 2, 500–504. https://doi.org/10.1038/NGEO557.

Stocchi, P., Vacchi, M., Lorscheid, T., de Boer, B., Simms, A.R., van der Wal, R.S.W., Verneersen, B.L.A., Pappalardo, M., Rovere, A., 2018. MIS 5e relative sea-level changes in the Mediterranean Sea: contribution of isostatic disequilibrium. Quat. Sci. Rev. 185, 122–135. https://doi.org/10.1016/j.quascirev.2018.01.004.

Villa, P., Boschian, G., Pollarolo, L., Saccà, D., Marra, F., Nomade, S., Pereira, A., 2021. Elephant bonesfor the Middle Pleistocene toolmaker. PLoS ONE 16 (8), e0256090. https://doi.org/10.1371/journal.pone.0256090.

Villa, P., Soriano, S., Grün, R., Marra, F., Nomade, S., Pereira, A., Boschian, G., Pollarolo, L., Fang, F., Bahain, J.J., 2016. The acheulian and early middle Paleolithic in Central Italy: stability and innovation. PLoS One 11 (8), e0160516. https://doi.org/10.1371/journal.pone.0160516.